CORTEX 63 (2015) 55–67

Available online at www.sciencedirect.com

ScienceDirect

Journal homepage: www.elsevier.com/locate/cortex

Research report

Resting state functional magnetic resonance imaging and neural network classified autism and control

Tetsuya Iidaka[*]

Department of Psychiatry, Graduate School of Medicine, Nagoya University, Nagoya, Aichi, Japan

ARTICLE INFO

Article history:
Received 3 February 2014
Reviewed 5 May 2014
Revised 2 June 2014
Accepted 12 August 2014
Action editor Mike Anderson
Published online 28 August 2014

Keywords:
Developmental disorder
Brain imaging
Diagnosis
Machine learning
Classifier

ABSTRACT

Although the neurodevelopmental and genetic underpinnings of autism spectrum disorder (ASD) have been investigated, the etiology of the disorder has remained elusive, and clinical diagnosis continues to rely on symptom-based criteria. In this study, to classify both control subjects and a large sample of patients with ASD, we used resting state functional magnetic resonance imaging (rs-fMRI) and a neural network. Imaging data from 312 subjects with ASD and 328 subjects with typical development was downloaded from the multi-center research project. Only subjects under 20 years of age were included in this analysis. Correlation matrices computed from rs-fMRI time-series data were entered into a probabilistic neural network (PNN) for classification. The PNN classified the two groups with approximately 90% accuracy (sensitivity = 92%, specificity = 87%). The accuracy of classification did not differ among the institutes, or with respect to experimental and imaging conditions, sex, handedness, or intellectual level. Medication status and degree of head movement did not affect accuracy values. The present study indicates that an intrinsic connectivity matrix produced from rs-fMRI data could yield a possible biomarker of ASD. These results support the view that altered network connectivity within the brain contributes to the neurobiology of ASD.

1. Introduction

Autism spectrum disorder (ASD) is characterized by the impaired development of social interaction and communication skills and a restricted repertoire of activities and interests (A.P.A., 1994). Although extensive efforts have been made to create a neurodevelopmental model (Baron-Cohen, 2009; Frith, 2001) and to identify disease-specific genes (Levy, Mandell, & Schultz, 2009), ASD continues to be diagnosed using symptom-based clinical criteria. The identification of biomarkers with clear neural underpinnings in ASD would be helpful in ensuring an early and accurate diagnosis as well as an optimally effective treatment (Hill & Frith, 2003; Levy et al., 2009). Structural and functional magnetic resonance imaging has the potential to reveal brain abnormalities of ASD that could be used as biomarkers of the disease.

* Department of Psychiatry, Graduate School of Medicine, Nagoya University, 65 Tsurumai, Showa, Nagoya, Aichi 466-8550, Japan.
E-mail address: iidaka@med.nagoya-u.ac.jp.
http://dx.doi.org/10.1016/j.cortex.2014.08.011
0010-9452/

A critical step in using neuroimaging abnormalities as biomarkers of ASD is applying a machine-learning algorithm such as the support vector machine (SVM) and/or an artificial neural network to the data (Orru, Pettersson-Yeo, Marquand, Sartori, & Mechelli, 2012). Structural properties of the brain, including cortical volume (Calderoni et al., 2012; Ecker, Rocha-Rego, et al., 2010; Uddin et al., 2011; Varol, Gaonkar, Erus, Schultz, & Davatzikos, 2012), thickness (Ecker, Marquand, et al., 2010; Jiao et al., 2011, 2010; Sato et al., 2013), and white matter integrity (Bloy et al., 2011; Ingalhalikar, Parker, Bloy, Roberts, & Verma, 2011), have been used as features to classify control subjects and patients with ASD; however, to date, these investigations have shown limited power of these measures as classifiers.

Investigating brain network activity during the resting state has emerged as a new method that eliminates the caveats of task-based fMRI studies (Menon, 2011). In this method, the fMRI signal is measured during the resting state and the data is analyzed based on a connectivity approach between subdivisions. To date, brain network activity during the resting state has been investigated in subjects with ASD and typical development in numerous studies (Assaf et al., 2010; Barttfeld et al., 2012; Cardinale, Shih, Fishman, Ford, & Muller, 2013; Di Martino et al., 2011; Di Martino, Zuo, et al., 2013; Ebisch et al., 2011; Lai et al., 2010; Lynch et al., 2013; Mueller et al., 2013; Murdaugh et al., 2012; Paakki et al., 2010; Tyszka, Kennedy, Paul, & Adolphs, 2014; Weng et al., 2010; Wiggins et al., 2011). Overall, intrinsic connectivity between subdivisions of the brain is altered in patients with ASD compared to controls (Muller et al., 2011; Uddin, Supekar, & Menon, 2010).

In studies that have used intrinsic connectivity during the resting state (Anderson et al., 2011; Barttfeld et al., 2012; Murdaugh et al., 2012) or during passive viewing of movies (Deshpande, Libero, Sreenivasan, Deshpande, & Kana, 2013) to classify ASD and control subjects, small sample sizes have limited the accuracy of the results. In a single study that used large samples from the same image database as the present study, the accuracy was as high as 60% (Nielsen et al., 2013). In the present study, using a large dataset ($n = 640$) obtained from the public database (Di Martino, Yan, et al., 2014) and a probabilistic neural network (PNN) algorithm, I report the successful classification of resting state fMRI data between subjects with ASD and subjects with typical development.

2. Materials and methods

2.1. Materials

The original imaging and demographic data were collected from the Autism Brain Imaging Data Exchange (ABIDE) database (http://fcon_1000.projects.nitrc.org/indi/abide/index.html), which allows unrestricted usage for non-commercial research purposes. Although the dataset included both adults and children, only subjects under 20 years of age were used in the present study. Brain images and related data from 312 subjects with ASD (male/female: 273/39) and 328 control subjects with typical development (CTL, male/female: 267/61) from 12 universities and research institutes were used. The names and abbreviations of these institutes and scanning parameters are listed in Table 1. The ethics committee of the Nagoya University School of Medicine approved the usage of this anonymous data for research purposes.

Autism was diagnosed according to both the Autism Diagnostic Interview-Revised (ADI-R) (Lord, Rutter, & Le Couteur, 1994) and the Autism Diagnostic Observation Schedule (ADOS) (Lord, Rutter, DiLavore, & Risi, 1999) in almost all cases, the exception being cases from one institute where autism was diagnosed using only the DSM-IV-TR (A.P.A., 1994). The CTL subjects were screened in clinical interviews conducted by experts in child psychiatry; however, in some cases, other questionnaires were used. The details of the diagnostic procedures and questionnaires used are listed in Supplementary Table 1.

Demographic data for each group is shown in Table 2. Subjects were aged between 6 and 19 years. The full-scale IQ of all subjects assessed was 41–148; however, no IQ data was available for three subjects with ASD. Between-group comparisons were made using unpaired *t*-tests (two-tailed) for age and IQ, and chi-square tests for sex and handedness (statistical threshold was set at $p = .05$). Data on the medication

Table 1 – Scanning parameters and experimental settings in each site.

Institute	MRI vendor	TR (msec)	TE (msec)	FA (deg)	Voxel size (mm)	Volumes	Time (m)	Eyes
KKI	Phillips	2500	30	75	3 × 3 × 3	156	6.5	o
LEU	Phillips	1667	33	90	3.48 × 3.59 × 4	250	6.9	c
NYU	Siemens	2000	15	90	3.75 × 3.75 × 4	180	6.0	o/c
OHSU	Siemens	2500	30	90	3.75 × 3.75 × 3.8	82	3.4	o
OLIN	Siemens	1500	27	60	3.43 × 3.43 × 4	210	5.3	o
PITT	Siemens	1500	25	70	3.12 × 3.12 × 4	200	5.0	c
SDSU	GE	2000	30	90	3.44 × 3.44 × 3.4	180	6.0	o
STAN	GE	2000	30	80	3.12 × 3.12 × 4.5	180	6.0	c
TRIN	Phillips	2000	28	90	3 × 3 × 3.5	150	5.0	c
UCLA	Siemens	3000	28	90	3 × 3 × 4	120	6.0	o
USM	Siemens	2000	28	90	3.43 × 3.43 × 3	240	8.0	o
YALE	Siemens	2000	25	60	3.43 × 3.43 × 4	200	6.7	o

KKI, Kennedy Krieger Institute; LEU, University of Leuven; NYU, NYU Langone Medical Center; OHSU, Oregon Health and Science University; OLIN, Olin, Institute of Living at Hartford Hospital; PITT, University of Pittsburgh School of Medicine; SDSU, San Diego State University; STAN, Stanford University; TRIN, Trinity Centre for Health Sciences; UCLA, University of California, Los Angeles; USM, University of Utah School of Medicine; YALE, Yale Child Study Center; FA; Flip angle, Time: Scan time, Eyes; eyes were open (o) or closed (c) during the scan.

Table 2 – Demographic data of the subjects.

	ASD	CTL	*p*-value
Number of subjects	312	328	N.A.
Mean age	13.2 (3.1)	12.9 (3.0)	.32
Male (%)	87.5	81.4	.03
Rt handedness (%)	84.3	91.8	.003
Mean full-scale IQ	103 (17)	110 (13)	.001

N.A., not available, SD in parenthesis.

status of the subjects were available from eight among the twelve sites (see Supplementary Table 2). Out of the 229 subjects with ASD investigated from these eight sites, 75 (24%) were and 152 (49%) were not receiving psychotropic medication at the time of scanning (data were not reported for two subjects). Medication status was unavailable for 83 of the ASD subjects (27%) investigated from the remaining four sites. The numbers of subjects and their demographic data from each institute are listed in Supplementary Table 2.

2.2. *Imaging data acquisition*

At each institute, functional brain images were acquired using a 3-T imager and a T2*-weighted gradient-echo echo-planar imaging (EPI) sequence, which is sensitive to blood oxygen level-dependent (BOLD) contrast. The subjects were asked to lie still in the scanner while remaining awake. Although the scanning parameters, MRI vendor, voxel size, number of volumes, scanning time, and instructions whether to keep eyes open/closed varied among the institutes, the general experimental procedure used was uniform within each institute. The number of image volumes taken for each subject ranged from 82 to 250 (mean = 179), and scanning time ranged from 3.4 min to 8.0 min (mean = 5.9 min). The details of the scanning parameters and experimental settings are provided in Table 1.

2.3. *Image data analysis*

2.3.1. *Preprocessing*

Data were analyzed using the SPM8 software (Wellcome Department of Imaging Neuroscience, London, UK, http://www.fil.ion.ucl.ac.uk/spm/) at the Department of Psychiatry, Nagoya University. After discarding the first five volumes, all volumes were spatially realigned to the mean volume, and the signal in each slice was temporally realigned to that obtained in the middle slice using sinc interpolation. The re-sliced volumes were normalized to the Montreal Neurological Institute (MNI) space with a voxel size of $3 \times 3 \times 3$ mm^3 using an EPI template of SPM8. The normalized images were spatially smoothed with a 4-mm Gaussian kernel. Head motion is known to have substantial effects on the results for functional connectivity (Van Dijk, Sabuncu, & Buckner, 2012). The root mean square (RMS) of six movement parameters along the time-series obtained in the realignment process was calculated for each subject (*x*-, *y*-, *z*-translation and *x*-, *y*-, *z*-rotation). The RMSs of the six head movement parameters for the two groups were subjected to unpaired *t*-tests (two-tailed, statistical threshold at $p = .05$). The means and S.E.s of these values for each group are shown in Fig. 1.

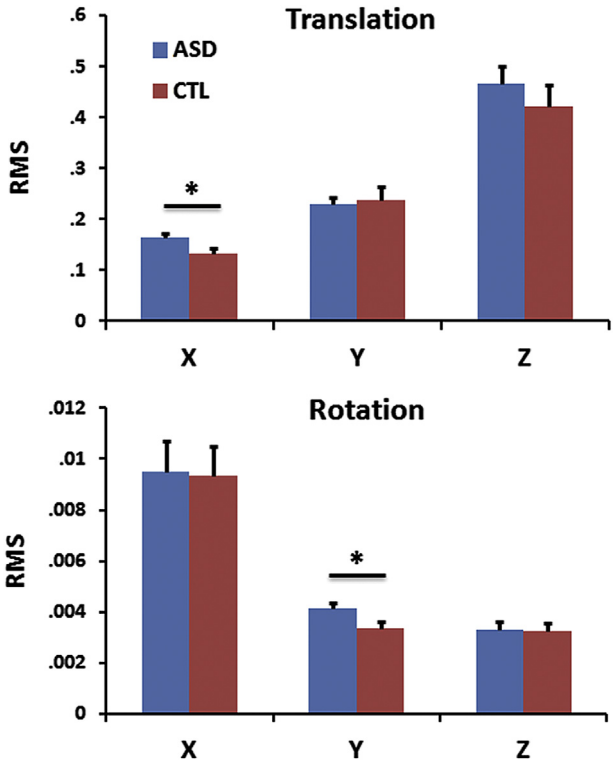

Fig. 1 – Top: The mean (column) and one S.E. (bar) of the root mean square (RMS) of translation parameters for each of the *x*-, *y*-, and *z*-axes obtained in the realignment process of SPM8. Blue columns represent the ASD group, and red columns represent the CTL group. There was a significant group difference in the *x*-axis, as indicated by a single asterisk ($p < .05$). Bottom: The mean (column) and one S.E. (bar) of the root mean square (RMS) of rotation parameters for each of the *x*-, *y*-, and *z*-axes obtained in the realignment process of SPM8. Blue columns represent the ASD group, and red columns represent the CTL group. There was a significant group difference in the *y*-axis, as indicated by a single asterisk ($p < .05$).

2.3.2. *Resting state functional connectivity analyses*

Resting state fMRI datasets were further processed using a toolkit of the Data Processing Assistant for Resting-State fMRI (DPARSF; http://www.rfmri.org) (Chao-Gan & Yu-Feng, 2010). Processing was conducted using the following steps: (1) removing the linear trend in the time series, (2) temporal band-pass filtering (.01–.08 Hz) to reduce the effect of low-frequency drift and high-frequency noise, and (3) controlling for non-neural noise in the time series by including covariates in the linear regression, i.e., six parameters from rigid body correction of head motion, the white matter signal, and the cerebrospinal fluid signal. The global mean signal was not removed in the present study (Fox, Zhang, Snyder, & Raichle, 2009; Murphy, Birn, Handwerker, Jones, & Bandettini, 2009).

Table 3 – Results of prediction accuracy: Leave-one-out cross validation.

Sensitivity	91.9%
Specificity	86.9%
Accuracy	89.4%
PPV	86.9%
NPV	91.9%
PPV_{corr}	7.4%
NPV_{corr}	99.9%

PPV, positive prediction value.
NPV, negative prediction value.
PPV_{corr}, corrected PPV.
NPV_{corr}, corrected NPV.

The residuals of the datasets after band-pass filtering and removal of the linear trend and eight covariates were considered as BOLD signal fluctuations originating from neuronal activity during the resting state. The Automated Anatomical Labeling (AAL) template (Tzourio-Mazoyer et al., 2002), which is widely used for identifying brain regions in the MNI space, was applied to the normalized and smoothed time-series datasets of each subject. The AAL template is a standard brain template for creating intrinsic connectivity (Lai et al., 2010; Supekar et al., 2013), although other templates, for example, the Harvard–Oxford Atlas (Di Martino, Yan, et al., 2014; Tyszka et al., 2014) and voxel-wise lattice method (Anderson et al., 2011; Nielsen et al., 2013) have been used for the same purpose. The AAL template divides each hemisphere into 45 distinct regions. The average time-series data were computed in each of the 90 regions for each subject. I used the AAL template because it is implemented in DPARSF software and a 90 × 90 correlation matrix is well suited to be entered into the classifier when considering the number of subjects and features. The names of these 90 regions are listed in Supplementary Table 3.

The time-series data from each of the 90 regions were cross-correlated, and Pearson's correlation coefficients (r) between each brain region and the remaining 89 regions were computed for each subject. Individuals' r values were normalized to z values using Fisher's z transformation. The z-transformed correlation coefficients were represented in a 90 × 90 matrix (8,100 cells), which was symmetric with regard to the diagonal. In the present study, the diagonal of the matrix was not valid and was not used for analysis. Therefore, the number of effective cells in the upper triangle of the matrix was 4,005. The mean and SD values of the correlation (z-transformed) matrices for the ASD and CTL groups were derived (only the mean matrices are shown in Fig. 2, left panel). Subsequently, the matrices representing the difference in mean correlation between the groups (Fig. 2, middle panel) and the standard deviation (not shown) were created. Finally, the matrix representing the effect size (Cohen's *d*) of the difference between the groups was

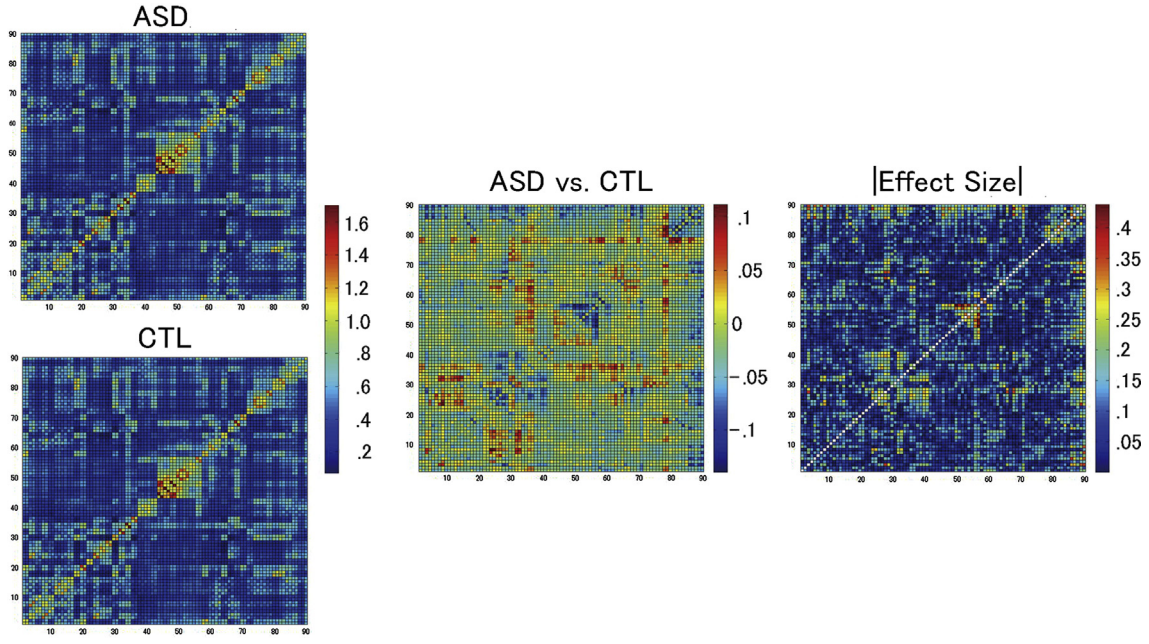

Fig. 2 – Left: Mean correlation matrices for the ASD (top, *n* = 312) and CTL (bottom, *n* = 328) groups during the resting state. The matrix represents 90 × 90 correlation coefficients of BOLD signal fluctuation between the subdivisions as defined by the AAL template. The color code indicates values of z-transformed correlation coefficients in each cell of the matrix. Middle: The difference correlation matrix between the ASD and CTL groups. The color code shows cells where subjects with ASD had greater correlations than CTL subjects in red, and cells where CTL subjects had greater correlations than subjects with ASD in blue. Right: The effect size (ES, Cohen's *d*) matrix of the difference between the ASD and CTL groups. The numerical values are absolute values. The matrix was computed from the matrices containing the differences and standard deviations of each group. The color code indicates higher ES in red and lower ES in blue. All the matrices were symmetric with respect to the diagonal, and the diagonal was invalid and was not used for analysis.

computed (Fig. 2, right panel shows matrix of absolute value of the effect size).

2.4. Classification between ASD and CTL

2.4.1. Procedure for feature selection

To search for an optimal threshold for the data to be entered into the classifier, the matrix was thresholded at seven different effect sizes (ESs, from .05 to .35 by .05 increments in absolute value). For example, at the threshold of .05 ES, 2,728 cells in the upper triangle of the matrix were used as features for the classifier. The numbers of features at each threshold are shown as columns in Fig. 3. Subsequently, z-transformed correlation coefficients of each of the 2,728 cells were extracted from the subject's original correlation matrix. The correlation data (numerical values of each cell) and diagnostic data (ASD or CTL, categorical label) were paired for each of the 640 subjects and entered into the classifier. The procedure was repeated at seven different thresholds of absolute ES.

2.4.2. PNN

A PNN (Specht, 1990) is an implementation of the kernel discriminant analysis statistical algorithm, which is organized into a multilayered feed forward neural network to perform classification. Recently, a PNN has been applied to physiological data measured by electroencephalogram (Sankari & Adeli, 2011; Ubeyli, 2008), pulse oximetry (Morillo & Gross, 2013), neuroimaging (Palumbo et al., 2010), and endoscopy (Pan, Yan, Qiu, & Cui, 2011), and has been successfully used in the classification of sample data into diseased and healthy states with high accuracy.

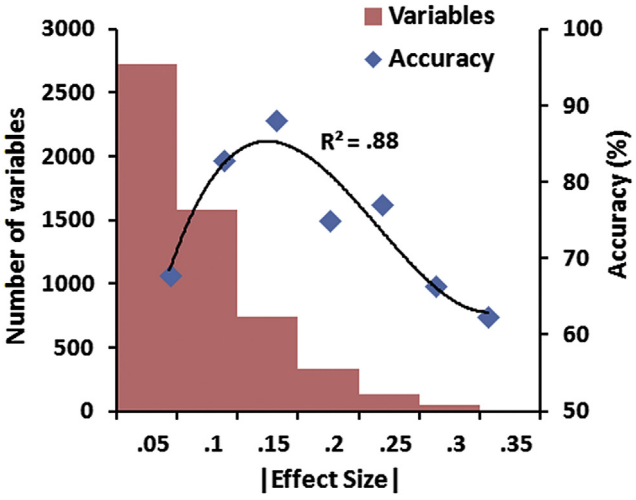

Fig. 3 – The vertical–left axis indicates the number of variables entered into the PNN and the vertical–right axis indicates the accuracy (%) of classification by the PNN. The horizontal axis indicates seven different ES thresholds. For example, at the threshold of ES = .1, the number of variables entered into PNN was 1,581, and the accuracy was 82.8%. The third degree polynomial regression line and r-square value for the accuracy data are shown.

The PNN classifier consists of four fully interconnected layers: an input layer, a pattern layer, a summation layer, and an output layer. The input layer has as many nodes as the number of features (i.e., number of cells in the matrix). The input layer nodes simply distribute input vectors to all the nodes in the pattern layer. The pattern layer has one node for each case in the training dataset (i.e., 640 cases or neurons). The pattern layer is fully connected to the input layer, with one node for each pattern in the datasets. Each node in the pattern layer receives the input vectors and estimates its probability density function, which was a Gaussian function in the present study. Here, a sigma value named as the "spread parameter" controls the size and shape of the Gaussian function. The optimal sigma values were estimated with the conjugate gradient algorithm. The jackknife method was used for evaluating the sigma values during the optimization process. The pattern layer outputs are selectively connected to nodes in the summation layer depending on the class of patterns (i.e., ASD and CTL). There is one node for each class, and each node sums the outputs from the pattern layer nodes. The output layer node yields a binary output value corresponding to the best subclass choice for the specific dataset based on the maximum probability or Bayes' rule. Thus, the final product of the PNN is a value of 1 for one class and 0 for the other. In the present study, DTREG (http://www.dtreg.com) was used to run the PNN (Sherrod, 2003).

On the other hand, SVM performs classification by constructing a multidimensional hyperplane that separates the data into two categories (target variables). A set of features that describes one case is called a vector (i.e., predictor variables). Therefore, the goal of SVM modeling is to find the optimal hyperplane that separates clusters of vectors in such a way that cases with one category of the target variable are on one side of the plane and cases with the other category are on the other side of the plane. The vectors near the hyperplane are called support vectors. The distance between the support vectors is called the margin. An SVM analysis finds the hyperplane that maximizes the margin between the support vectors. In a high dimensional space, SVM uses a kernel function to map the data into a different space where a hyperplane can be used to separate the data (Sherrod, 2003). Several studies have found that PNN and SVM yielded comparable accuracy levels for classifying biological data (Loukas et al., 2013; Muniz et al., 2010); however, the PNN had advantages in the processing speed (Specht, 1990).

To explore an optimal set of feature variables, datasets at seven different ESs were entered individually into the PNN, and the prediction accuracy was computed by using leave-one-out cross-validation (LOOCV). In LOOCV, one subject's data are left out of the dataset, and the neural network creates an optimal classifier using the remaining data. The classifier predicts the label (ASD or CTL) of the one subject who was left out, and the accuracy of this prediction is assessed. This procedure was repeated as many times as the number of subjects, with a different subject being left out each time; finally, total accuracy was computed for each category. The prediction data included true positive (TP), false negative (FN), true negative (TN), and false positive (FP) classifications. The

sensitivity, specificity, accuracy, positive prediction value (PPV), and negative prediction value (NPV) were computed using the following formulas:

$$\text{Sensitivity} = \text{TP}/(\text{TP} + \text{FN})*100$$

$$\text{Specificity} = \text{TN}/(\text{TN} + \text{FP})*100$$

$$\text{Accuracy} = (\text{TP} + \text{TN})/(\text{TP} + \text{TN} + \text{FP} + \text{FN})*100$$

$$\text{PPV} = \text{TP}/(\text{TP} + \text{FP})*100$$

$$\text{NPV} = \text{TN}/(\text{TN} + \text{FN})*100$$

However, the PPV and NPV computed by the formulas above do not provide a realistic picture of the prediction value because they depend critically on the prevalence of the disorder in the general population (Castellanos, Di Martino, Craddock, Mehta, & Milham, 2013). Accordingly, these values were adjusted accounting for recent estimates of disorder prevalence from the Centers for Disease Control and Prevention, Morbidity and Mortality Weekly Report in 2012 (C.D.C.P., 2012). The corrected PPV and NPV were computed using the following formulas (Altman & Bland, 1994):

$$\text{PPV}_{\text{corr}} = \frac{\text{sensitivity}*\text{prevalence}}{\text{sensitivity}*\text{prevalence} + (1 - \text{specificity})*(1 - \text{prevalence})}$$

$$\text{NPV}_{\text{corr}} = \frac{\text{specificity}*(1 - \text{prevalence})}{\text{specificity}*(1 - \text{prevalence}) + (1 - \text{sensitivity})*\text{prevalence}}$$

The disease prevalence was .0113 according to the report noted above (C.D.C.P., 2012).

For the datasets at seven different ESs, the accuracy for the combined ASD and CTL groups was plotted in Fig. 3. Seven plots of accuracy data were fitted by a polynomial (3rd degree) function curve; consequently, it appeared that the optimal ES threshold existed within the range of .1–.2. Finally, the LOOCV procedure was repeated using datasets thresholded at absolute ES values ranging from .1 to .2 by .01 increments in an effort to determine the highest prediction accuracy. For the best prediction data, i.e., the dataset with the highest accuracy when the absolute value of ES was varied from .1 to .2, the ES (not the absolute value) matrix and lobar/region names are illustrated in Fig. 4.

2.4.3. *Other validation methods*

To confirm the reliability of the results of LOOCV, V-fold cross-validation (CV) of PNN was conducted by using the same correlation matrices of 640 subjects as those entered into the LOOCV. In a V-fold CV, a model was constructed with (V−1)/V proportion of the subjects being used. The selection of the subjects occurred randomly each time. The validation of a remaining set of subjects (1/V proportion of subjects) was performed using the constructed model. I conducted 2-, 10-, and 50-fold CVs. The validation results in each model are shown in Table 4.

2.5. *Effect of confounding factors*

2.5.1. *Effects of potentially confounding factors on accuracy*

Because the PNN was conducted on a dataset of 640 subjects from 12 institutes, variations of imaging and experimental protocols could artifactually alter the present results. To investigate whether the prediction accuracy was confounded by such factors, my accuracy data was compared across institutes, MRI vendors, eyes open/closed conditions, sex, age, handedness, and full-scale IQ groups (Fig. 5). For age, accuracy was compared among three groups (under 10 years old, $n = 119$; 10–15 years old, $n = 350$; and 15–20 years old, $n = 171$). For full-scale IQ values, the means ± 1 SD were used as cut-off points (under 91, $n = 105$; 92 to 121, $n = 417$; and over 122, $n = 115$). Chi-square tests were used for these analyses (statistical threshold was set at $p = .05$).

2.5.2. *Effects of medication and head movement on accuracy*

To investigate whether medication status affected prediction accuracy, chi-square tests were conducted for the three ASD groups (on-medication, off-medication, and no data). For analyzing the relationship between head movements and accuracy data, all 640 subjects were sorted according to the RMS value of head movement parameters and divided into 10 bins with 64 subjects each. The accuracy data was computed for each of the 10 bins and compared using chi-square tests. Data of x-translation and y-rotation were used for this analysis because significant group differences were obtained only for these two measures (see Results and Fig. 6). The statistical threshold of chi-square tests was set at $p = .05$.

2.5.3. *Characteristics of the false-negative group*

From a clinical point of view, the characteristics of subjects who had ASD but were incorrectly classified as having "typical development" (FN) are particularly important. Therefore, the proportion of sex and handedness, mean age, and mean and skewness of full-scale IQ were compared between the four classification groups (TP, FN, FP, and TN). In addition, the total score of ADOS (if ADOS was not available and total score of ADOS-Gotham was available, the latter was used) was compared between the TP (ADOS total score, 247 subjects; ADOS-Gotham total score, 23 subjects; no data, 17 subjects) and FN (ADOS total score, 18 subjects; ADOS-Gotham total score; 4 subjects; no data, 3 subjects) groups. For numerical variables other than skewness, one-way ANOVA was conducted (threshold was set at $p = .05$ after multiple comparisons with Fisher's least square method). The chi-square test was used to analyze the categorical variables (threshold was set at $p = .05$). These data are plotted in Fig. 7.

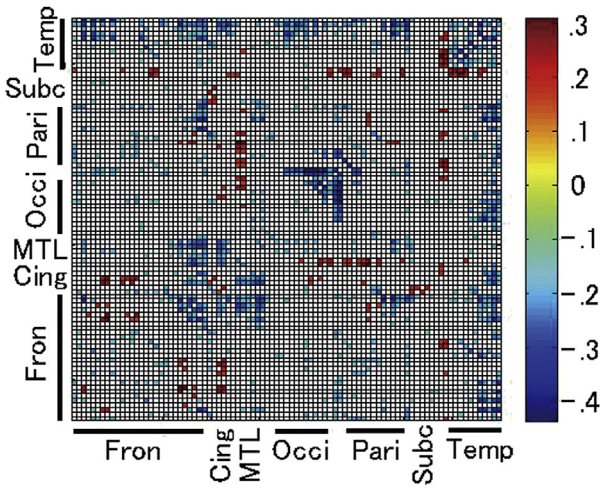

Fig. 4 – Effect size matrix between the groups at the absolute value threshold of .16. The cells that had ES greater than .16 or smaller than −.16 are shown in color, and all other cells are blank. The matrix best predicted the diagnostic labels at 89.4% accuracy. Red cells indicate a greater correlation in the ASD group than in the CTL group, and blue cells indicate a greater correlation in the CTL than in the ASD group. Lobar/region names are roughly indicated in each axis. The order of region from the origin (left-bottom point of matrix) is the same as in the AAL notation. Fron, frontal lobe; Cing, cingulate cortex; MTL, medial temporal lobe; Occi, occipital lobe; Pari, parietal lobe; Subc, subcortical nuclei; Temp, temporal lobe.

3. Results

3.1. *Subjects' characteristics*

Mean age did not significantly differ between the ASD and CTL group ($t = .98$, df = 638, $p = .32$). The percentage of male subjects was significantly higher in the ASD than in the CTL group (chi-square = 4.5, df = 1, $p = .03$) and the percentage of right-handed subjects was lower in the ASD than in the CTL group (chi-square = 8.5, df = 1, $p = .003$). Mean full-scale IQ was significantly lower in the ASD than in the CTL group ($t = 5.65$, df = 635, $p < .001$).

Table 4 – Results of prediction accuracy: V-fold cross validation.

	2-fold	10-fold	50-fold
Sensitivity	75.0%	85.9%	92.3%
Specificity	79.3%	87.8%	88.4%
Accuracy	77.2%	86.9%	90.3%
PPV	77.5%	87.0%	88.3%
NPV	76.9%	86.7%	92.4%
PPV_{corr}	3.9%	7.5%	8.3%
NPV_{corr}	99.6%	99.8%	99.9%

PPV, positive prediction value.
NPV, negative prediction value.
PPV_{corr}, corrected PPV.
NPV_{corr}, corrected NPV.

3.2. *Differences in head movement parameters between the groups*

For the translation parameters obtained during the realignment process, a significant difference was observed in the x-axis ($t = 2.23$, df = 638, $p = .02$), but not in the y-axis ($t = .28$, df = 638, $p = .78$) or z-axis ($t = .82$, df = 638, $p = .41$). For rotation parameters, there was a significant difference in the y-axis ($t = 2.32$, df = 638, $p = .02$), but not in the x-axis ($t = .13$, df = 638, $p = .89$) or z-axis ($t = .17$, df = 638, $p = .86$). Overall, the means of the RMS parameter were greater in the ASD group than in the CTL group.

3.3. *Leave-one-out cross validation and V-fold cross validation by the PNN*

For the datasets at seven different ESs, the accuracy for the combined ASD and CTL groups ranged from 62.5 (ES = .35) to 88.1 (ES = .15), as plotted in Fig. 3. Seven plots of accuracy data were effectively fitted by a polynomial (3rd degree) function curve with the r-square value of .88. The LOOCV procedure repeated at absolute ES ranging from .1 to .2 by .01 increments revealed that the absolute ES of .16 produced the best prediction accuracy. At this threshold, there were 632 cells in the matrix. The numbers of TP, FN, TN, and FP cases were 287, 25, 285, and 43, respectively. The sensitivity, specificity, accuracy, PPV, NPV, PPV_{corr}, and NPV_{corr} are shown in Table 3. The results of V-fold CV shown in Table 4 indicate that the accuracy obtained by 10- and 50-fold CVs achieved the same level of accuracy as with the LOOCV; however, the 2-fold CV was less accurate than the LOOCV.

3.4. *Visualization of the matrix and network analysis*

The matrix that best classified the two groups (Fig. 4) had cells with both positive (92 cells, maximum = .307, shown in red) and negative (540 cells, minimum = −.437, shown in blue) values. A positive cell indicates regional connectivity where subjects with ASD had greater values than CTL subjects, and a negative cell indicates regional connectivity where CTL subjects had greater values than subjects with ASD. The positive cells were located in restricted regions such as the bilateral medial parts of the superior frontal gyrus (Frontal_Sup_Medial, N.B. AAL notation), anterior and posterior parts of the cingulate gyrus (Cingulum_Ant, Cingulum_Post), and thalamus (Thalamus). In contrast, the negative cells were widely distributed throughout the brain, but showed a tendency to cluster in the temporal and frontal lobes.

3.5. *Effects of confounding factors on accuracy*

No significant differences in accuracy were obtained for the different institutes from where study data were collected (chi-square = 9.53, df = 11, $p = .57$); likewise, factors including MRI vendor (chi-square = .63, df = 2, $p = .73$), sex (chi-square = 1.64, df = 1, $p = .20$), age (chi-square = 3.41, df = 2, $p = .18$), handedness (chi-square = .18, df = 1, $p = .67$), IQ (chi-square = 2.36, df = 2, $p = .31$), or eye condition (open/closed; chi-square = .04, df = 1, $p = .83$) did not show any effects on the accuracy. The accuracy data for each factor is shown in Fig. 5.

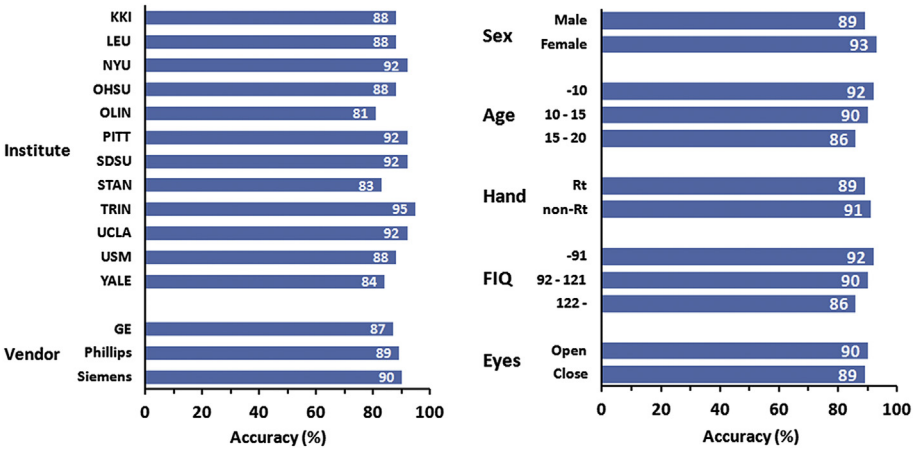

Fig. 5 – The column indicates mean accuracy computed for each institute (left), MRI vendor (left), sex (right), age (right), handedness (right), full-scale IQ (right), and eye condition (right). The numerical value on each column indicates accuracy (%). There were no significant differences in accuracy between the potentially confounding factors. For statistical results, see the Results section.

3.6. *Effects of medication and head movement on accuracy*

The accuracy values for the on-medication, off-medication, and no-data groups were 89.3, 95.4, and 88.2, respectively; these groups did not show any significant differences in accuracy (chi-square = 4.73, df = 2, p = .09). Regarding head movement parameters, there was no effect of x-translation (chi-square = 14.1, df = 9, p = .12) or y-rotation (chi-square = 5.19, df = 9, p = .82) on accuracy data. The data for each bin are shown in Fig. 6.

3.7. *Characteristics of the false-negative group*

There were significant differences in mean age [SD] among the four classification groups (TP: 13.0 [3.1], FN: 14.8 [2.9], TN: 12.9 [2.9], FP: 12.6 [2.9]; $F_{(3, 639)} = 2.99$, p = .03). Specifically, as revealed by multiple comparison analysis, the FN group was older than the other groups (Fig. 7, left panel). There was also a significant difference in mean IQ [SD] among the groups (TP: 102 [17], FN: 111 [17], TN: 110 [12], FP: 109 [14]; $F_{(3, 636)} = 13.34$, p = .001); in this case, the TP group had the lowest IQ values (Fig. 7, middle panel). Skewness of IQ data in each group was .1, −.37, −.19, and −.15 for TP, FN, TN, and FP, respectively. The proportion of male subjects did not differ among the groups (TP: 86%, FN: 96%, TN: 80%, FP: 86%; chi-square = 6.81, df = 3, p = .08). The proportion of right-handedness significantly differed among the groups (TP: 83%, FN: 92%, TN: 92%, FP: 88%; chi-square = 10.62, df = 3, p = .01). Finally, the mean total ADOS score did not differ between the TP and FN groups ($F_{(1, 291)} = .19$, p = .66; TP: 11.3 [3.8], FN: 11.4 [4.2]; Fig. 7, right panel). There were no

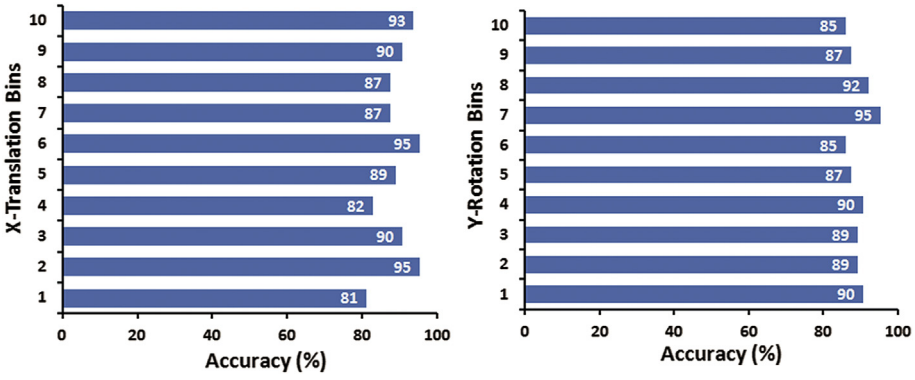

Fig. 6 – The columns indicate mean accuracy computed for each subgroup divided by the parameters indicating the degree of head movement. All 640 subjects were sorted according to the RMS of head movement parameters and divided into 10 subgroups with 64 subjects in each. Numbers on the vertical axis indicate subgroups, ranging from 1, with the largest mean RMS, to 10, with the smallest mean RMS. Only the results for *x*-translation and *y*-rotation are shown because only these parameters showed significant differences between the groups. The numerical value on each column indicates accuracy (%). There was no significant effect of head movements on data accuracy. For statistical results, see the Results section.

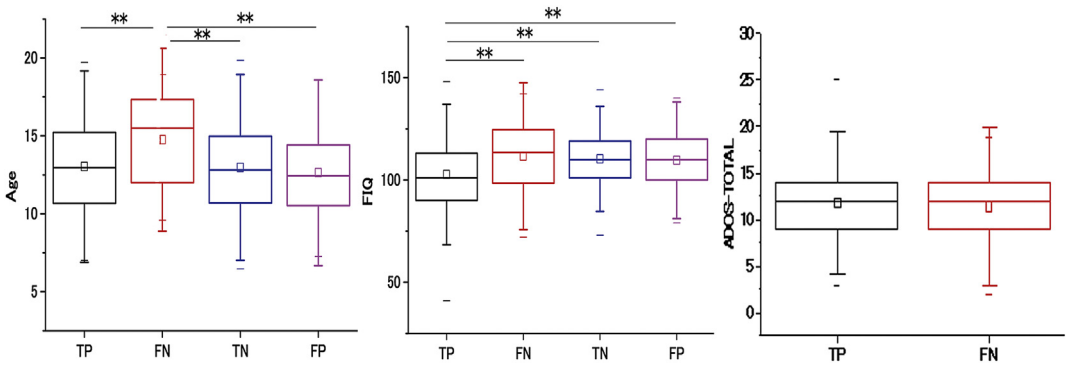

Fig. 7 – Box-plot graphs for the four prediction groups (TP: true positive; FN: false negative; TN: true negative; FP: false positive). Boxes represent the median values, and 25th and 75th percentile values. Squares and bars represent mean and maximum/minimum values, respectively. A double asterisk indicates statistical significance at $p < .01$ after multiple comparison analyses. Left: Mean age was significantly greater for the FN group than for other groups ($p < .01$). Middle: Mean full-scale IQ was significantly lower for the TP group than for other groups ($p < .01$). Right: The mean total ADOS score did not significantly differ between the TP and FN groups.

significant correlations between age, IQ, and ADOS scores within the FN group (all p values > .2).

4. Discussion

Correlation matrices created from resting state fMRI time-series data were classified as ASD or CTL with approximately 90% accuracy using the PNN algorithm. The present study revealed a potential diagnostic biomarker of ASD using a large data set ($n = 640$); importantly, this biomarker can be assigned with both high sensitivity (92%) and high specificity (87%). There was no significant difference in accuracy due to differences in institutes, scanners, imaging parameters, experimental protocols, age, or intellectual level. Likewise, the medication status and degree of head motion did not have significant effects on accuracy. Visualization of the best prediction matrix revealed that both hypo- and hyper-connectivity between subdivisions in the brain are critical for the successful classification of subjects into categories of typical and atypical development. The analytic procedure employed in the present study represents an entirely hypothesis-free, data-driven approach and should be replicable by any researcher.

In a previous study using a functional connectivity matrix, 40 subjects with ASD and 40 subjects with typical development were classified with as high as 79% accuracy (Anderson et al., 2011). Importantly, as shown in the present study, the subjects who were under 20 years of age were more accurately classified (89%). In another study that used SVM and intrinsic connectivity analysis, the difference matrix between the task conditions was used to identify features of ASD (Barttfeld et al., 2012). The accuracy of classification between patients with ASD ($n = 12$) and control subjects ($n = 12$) was as high as 91% in that investigation. Another study used a matrix obtained during the resting state with the AAL template to classify patients with ASD ($n = 13$) and control ($n = 14$) subjects at 78% accuracy (Murdaugh et al., 2012). Activity in salience network as revealed by independent component analysis classified subjects with ASD ($n = 20$) and typical development ($n = 20$) with 78% accuracy (Uddin, Supekar, Lynch, et al., 2013). Although these studies attained relatively high classification accuracy, the numbers of subjects in these studies were small, and thus, the results were required to be validated in larger samples.

In a single study that used the ABIDE database, the classification procedure attained only 60% accuracy (Nielsen et al., 2013), showing less accuracy than the present study. In that study, imaging data of adult subjects were included and the number of subdivisions of the brain was much larger than in the present study (90 *vs* 7,266 regions). Furthermore, the classification algorithm differed from the present study (PNN *vs* general linear model). These differences in methodology might account for the differences in classification accuracy between the studies. It is suggested that PNN could be a better choice to classify the intrinsic connectivity of neuroimaging data. The accuracy level of the LOOCV was replicated by using the 10-fold CV, which is a standard validation method of machine-learning algorithms including PNN, SVM, and multilayer perceptron. While the accuracy of 2-fold CV (77%) was less than the other CVs, it was still more accurate that using a general linear model with data from the same database (60%) (Nielsen et al., 2013).

Interestingly, I observed no significant differences in accuracy among the institutes where the original data was collected, or as a function of MRI vendor, or for the subgroups of age, sex, or intellectual level. These confounding variables have been major limiting factors to conducting multi-center projects (Yendiki et al., 2010). Thus, the present analytical procedure had a discriminant power with regard to childhood and adolescent subjects with ASD and could be applied to large data sets. Furthermore, the absence of a significant effect of medication status or head motion on accuracy data is critical for the use of the present method in a clinical setting since discontinuation of medication is often difficult and excluding data of patients with head movement reduces sample size and statistical power.

The subjects with ASD who were incorrectly classified as subjects with typical development (FN group) in the present study had similar total ADOS scores to subjects in the correctly classified (TP) group. However, the mean full-IQ of the FN group was significantly higher than that of the TP group and was almost comparable with that of the CTL group. In the FN group, the IQ data was skewed to the left, i.e., the distribution of IQ deviated to a higher range as compared with the TP group that showed a relatively symmetrical distribution. Therefore, the FN group had a similar intellectual level to the CTL group but similar degrees of autistic symptoms to the TP group. The results suggest that the FN and TP groups may have differential biological underpinnings in terms of intelligence and functional brain connectivity. Particularly, the PNN classifier would be more accurate in patients who have middle-range IQ than in those with high IQ. For those who have low IQ (<70), it is uncertain that the PNN classifier works effectively because only five ASD subjects had IQ lower than 70 in the present data set. Further research is needed to fully elucidate the biological underpinnings of ASD by incorporating clinical features and rs-fMRI connectivity analysis.

In the matrix that best classified the groups (Fig. 4), there were 5.8-fold more negative cells (85.4%) than positive cells (14.6%). This indicates that the major discriminatory factor between ASD and CTL subjects is hypoconnectivity within the network, although hyperconnected regions could not be disregarded. These results are in accordance with previous findings obtained using rs-fMRI (Assaf et al., 2010; Barttfeld et al., 2012; Cardinale et al., 2013; Di Martino et al., 2011; Di Martino, Zuo, et al., 2013; Ebisch et al., 2011; Lai et al., 2010; Lynch et al., 2013; Mueller et al., 2013; Murdaugh et al., 2012; Paakki et al., 2010; Tyszka et al., 2014; Weng et al., 2010; Wiggins et al., 2011), which showed both decreased and increased connectivities between subdivisions of the brain in patients with ASD compared to controls (Muller et al., 2011; Uddin et al., 2010). In those studies, critical regions with hypoconnectivity were distributed widely throughout the brain and could not be summarized into one or several discrete networks. A similar situation is evident in the present study. Because the spatial distribution of positive cells is more localized than that of negative cells, it would be useful to more thoroughly investigate cells with hyperconnectivity as well as those with hypoconnectivity to clearly elucidate the neurobiology of ASD.

In the present study, intrinsic connectivity from particular regions, i.e., the medial part of the superior frontal gyrus, anterior and posterior cingulate cortices, and thalamus, to other brain regions was greater in subjects with ASD than in CTL subjects. Interestingly, several previous studies on children with ASD have similarly shown hyperconnectivity between subdivisions of the brain during rs-fMRI (Di Martino et al., 2011; Di Martino, Zuo, et al., 2013; Lynch et al., 2013; Uddin, Supekar, Lynch, et al., 2013). Compared to controls, subjects with ASD are reported to have increased connectivity in the caudate and putamen and in the bilateral insulae and temporo-parietal lobes (Di Martino et al., 2011). Children with ASD also showed greater connectivity of the posterior cingulate cortex with regions in the temporo-occipital lobes and parahippocampal gyrus (Lynch et al., 2013). The hyperconnectivity in ASD encompassed several networks of the brain as revealed by independent component analysis (Uddin, Supekar, Lynch, et al., 2013). Furthermore, results obtained from the same database as the present study revealed ASD-related hyperconnectivity, which was limited to subcortical regions, particularly between the thalamus/globus pallidus and sensorimotor regions (Di Martino, Yan, et al., 2014). Therefore, hyperconnectivity between brain regions may be a specific biomarker of ASD in children and adolescents. Investigating thalamo-cortical networks in these subjects could thus help elucidate the pathogenesis of the disorder.

In addition, several recent studies using child and adolescent participants showed that connectivity as measured by rs-fMRI was significantly higher in subjects with ASD than in subjects with typical development. The degree of local and short-range connectivity in the occipital cortical areas was significantly lower in ASD than in controls and had a positive correlation with symptom severity in the patient group (Keown et al., 2013). In the study that used participants of 7–13 years, long-range connectivity in the primary sensory, paralimbic, and association areas as well as connectivity between these areas were higher in ASD than in controls (Supekar et al., 2013). In accord with these studies, it is hypothesized that intrinsic connectivity of the brain may differ between child, adolescent, and adult subjects (Uddin, Supekar, & Menon, 2013). In their model, connectivity in late adolescents and adults with ASD was generally reduced as compared with age-matched controls, and connectivity in children and early adolescents with the disorder appears to be increased. Therefore, investigation of age-related changes in brain connectivity using a dataset divided into several different age groups is necessary in the future.

The present study has several caveats. Detailed characteristics of the subjects were not available because the original data were collected at each institute independently. Thus, it is possible that the same subject was tested more than once at different institutes or on more than one occasion. Although male and female subjects showed a similar level of accuracy in the present study, further study is needed to investigate possible sex differences in intrinsic connectivity using an independent sample of female subjects. Another potential limitation is that the same brain template was used to obtain imaging data from every subject, despite the wide range of subjects' ages. In addition, use of a single brain template (e.g., ALL) in the present study might be insufficient to obtain replicable results of functional connectivity across whole brain regions. In future studies, analyses using several different ROIs or voxel-level templates should be compared to replicate the accuracy of classification.

Although the head motion parameters have been used as regressors before computing the correlation matrix in the present study, it might be insufficient to completely remove those confounding effects. Potentially other confounding factors such as imaging and experimental protocols could not be controlled in the data analysis; consequently, the effects of such factors on accuracy were tested *post hoc*. Furthermore, the classification results might be, at least to some degree, attributable to differences in subjects' motion, attention, anxiety, thought content, or other physiological factors during scanning, which may differ between the ASD and CTL groups. Thus far, such difficulties have not been solved in research

efforts involving multiple institutes and datasets with a large sample size, and further effort will be needed to address these issues.

Although the present study achieved high prediction accuracy, the corrected PPV will not be close to 100% even if both the sensitivity and specificity are high when the disease prevalence is very low. Therefore, in screening the general population, the best performing classifier for diagnosis will most likely model healthy individuals rather than patients. Finally, it is premature to suggest that the intrinsic connectivity matrix could be a specific biomarker of ASD because the present study used only groups of ASD and typical development and no other neurodevelopmental disorder such as ADHD.

In conclusion, an intrinsic connectivity matrix computed using rs-fMRI time-series data and a PNN algorithm successfully classified children and adolescents with ASD and those with typical development. A major achievement of this study is the high classification accuracy achieved using neuroimaging data for a large sample size collected from different institutes, in spite of the existence of several confounding factors. The analytical method developed here is a simple, hypothesis-free, and data-driven approach, and the study can be replicated using a similar publically available database. The present study contributes not only to research for a possible biomarker of ASD, but also to our general understanding of the biological underpinnings of this developmental disorder. By adding different samples to the present dataset and by repeating the analytical procedures, brain networks involved in the pathogenesis of ASD may be clarified in the future.

Funding

This study was supported by KAKENHI 21220005.

Competing financial interests

The author declares no competing financial interests.

Acknowledgments

The author thanks all researchers and funding agencies contributed to ABIDE. The names of institutes and their funding sources included in the database are listed in Supplementary Table 4. The author also thanks Maeri Yamamoto and Akiko Hayashi for their help in data preparation. Software programming and development were supported by Medical Try System, Kodaira, Japan.

Supplementary data

Supplementary data related to this article can be found at http://dx.doi.org/10.1016/j.cortex.2014.08.011.

REFERENCES

Altman, D. G., & Bland, J. M. (1994). Diagnostic tests 2: predictive values. *British Medical Journal, 309*, 102.

Anderson, J. S., Nielsen, J. A., Froehlich, A. L., DuBray, M. B., Druzgal, T. J., Cariello, A. N., et al. (2011). Functional connectivity magnetic resonance imaging classification of autism. *Brain, 134*, 3742–3754.

A.P.A. (1994). *Diagnostic and statistical manual for mental disorders* (4th ed.) (Text Revision).

Assaf, M., Jagannathan, K., Calhoun, V. D., Miller, L., Stevens, M. C., Sahl, R., et al. (2010). Abnormal functional connectivity of default mode sub-networks in autism spectrum disorder patients. *NeuroImage, 53*, 247–256.

Baron-Cohen, S. (2009). Autism: the empathizing-systemizing (E-S) theory. *Annals of the New York Academy of Sciences, 1156*, 68–80.

Barttfeld, P., Wicker, B., Cukier, S., Navarta, S., Lew, S., Leiguarda, R., et al. (2012). State-dependent changes of connectivity patterns and functional brain network topology in autism spectrum disorder. *Neuropsychologia, 50*, 3653–3662.

Bloy, L., Ingalhalikar, M., Eavani, H., Roberts, T. P., Schultz, R. T., & Verma, R. (2011). HARDI based pattern classifiers for the identification of white matter pathologies. *Medical Image Computing and Computer Assisted Intervention, 14*, 234–241.

Calderoni, S., Retico, A., Biagi, L., Tancredi, R., Muratori, F., & Tosetti, M. (2012). Female children with autism spectrum disorder: an insight from mass-univariate and pattern classification analyses. *NeuroImage, 59*, 1013–1022.

Cardinale, R. C., Shih, P., Fishman, I., Ford, L. M., & Muller, R. A. (2013). Pervasive rightward asymmetry shifts of functional networks in autism spectrum disorder. *JAMA Psychiatry, 70*, 975–982.

Castellanos, F. X., Di Martino, A., Craddock, R. C., Mehta, A. D., & Milham, M. P. (2013). Clinical applications of the functional connectome. *NeuroImage, 80*, 527–540.

C.D.C.P. (2012). *Modbidity and mortality weekly report*. Centers for Disease Control and Prevention.

Chao-Gan, Y., & Yu-Feng, Z. (2010). DPARSF: a MATLAB Toolbox for "Pipeline" data analysis of resting-state fMRI. *Frontiers in Systems Neuroscience, 4*, 13.

Deshpande, G., Libero, L. E., Sreenivasan, K. R., Deshpande, H. D., & Kana, R. K. (2013). Identification of neural connectivity signatures of autism using machine learning. *Frontiers in Human Neuroscience, 7*, 670.

Di Martino, A., Kelly, C., Grzadzinski, R., Zuo, X. N., Mennes, M., Mairena, M. A., et al. (2011). Aberrant striatal functional connectivity in children with autism. *Biological Psychiatry, 69*, 847–856.

Di Martino, A., Yan, C. G., Li, Q., Denio, E., Castellanos, F. X., Alaerts, K., et al. (2014). The autism brain imaging data exchange: towards a large-scale evaluation of the intrinsic brain architecture in autism. *Molecular Psychiatry, 19*, 659–667a.

Di Martino, A., Zuo, X. N., Kelly, C., Grzadzinski, R., Mennes, M., Schvarcz, A., et al. (2013). Shared and distinct intrinsic functional network centrality in autism and attention-deficit/hyperactivity disorder. *Biological Psychiatry, 74*, 623–632b.

Ebisch, S. J., Gallese, V., Willems, R. M., Mantini, D., Groen, W. B., Romani, G. L., et al. (2011). Altered intrinsic functional connectivity of anterior and posterior insula regions in high-functioning participants with autism spectrum disorder. *Human Brain Mapping, 32*, 1013–1028.

Ecker, C., Marquand, A., Mourao-Miranda, J., Johnston, P., Daly, E. M., Brammer, M. J., et al. (2010a). Describing the brain in autism in five dimensions–magnetic resonance imaging-

assisted diagnosis of autism spectrum disorder using a multiparameter classification approach. *Journal of Neuroscience, 30*, 10612–10623.
Ecker, C., Rocha-Rego, V., Johnston, P., Mourao-Miranda, J., Marquand, A., Daly, E. M., et al. (2010b). Investigating the predictive value of whole-brain structural MR scans in autism: a pattern classification approach. *NeuroImage, 49*, 44–56.
Fox, M. D., Zhang, D., Snyder, A. Z., & Raichle, M. E. (2009). The global signal and observed anticorrelated resting state brain networks. *Journal of Neurophysiology, 101*, 3270–3283.
Frith, U. (2001). Mind blindness and the brain in autism. *Neuron, 32*, 969–979.
Hill, E. L., & Frith, U. (2003). Understanding autism: insights from mind and brain. *Philosophical Transactions of the Royal Society London B Biological Sciences, 358*, 281–289.
Ingalhalikar, M., Parker, D., Bloy, L., Roberts, T. P., & Verma, R. (2011). Diffusion based abnormality markers of pathology: toward learned diagnostic prediction of ASD. *NeuroImage, 57*, 918–927.
Jiao, Y., Chen, R., Ke, X., Cheng, L., Chu, K., Lu, Z., et al. (2011). Predictive models for subtypes of autism spectrum disorder based on single-nucleotide polymorphisms and magnetic resonance imaging. *Advances in Medical Sciences, 56*, 334–342.
Jiao, Y., Chen, R., Ke, X., Chu, K., Lu, Z., & Herskovits, E. H. (2010). Predictive models of autism spectrum disorder based on brain regional cortical thickness. *NeuroImage, 50*, 589–599.
Keown, C. L., Shih, P., Nair, A., Peterson, N., Mulvey, M. E., & Muller, R. A. (2013). Local functional overconnectivity in posterior brain regions is associated with symptom severity in autism spectrum disorders. *Cell Reports, 5*, 567–572.
Lai, M. C., Lombardo, M. V., Chakrabarti, B., Sadek, S. A., Pasco, G., Wheelwright, S. J., et al. (2010). A shift to randomness of brain oscillations in people with autism. *Biological Psychiatry, 68*, 1092–1099.
Levy, S. E., Mandell, D. S., & Schultz, R. T. (2009). Autism. *Lancet, 374*, 1627–1638.
Lord, C., Rutter, M., DiLavore, P. C., & Risi, S. (1999). *Autism diagnostic observation schedule*. Los Angeles: Western Psychological Service.
Lord, C., Rutter, M., & Le Couteur, A. (1994). Autism diagnostic interview-revised: a revised version of a diagnostic interview for caregivers of individuals with possible pervasive developmental disorders. *Journal of Autism and Developmental Disorders, 24*, 659–685.
Loukas, C., Kostopoulos, S., Tanoglidi, A., Glotsos, D., Sfikas, C., & Cavouras, D. (2013). Breast cancer characterization based on image classification of tissue sections visualized under low magnification. *Computational and Mathematical Methods in Medicine, 2013*, 829461.
Lynch, C. J., Uddin, L. Q., Supekar, K., Khouzam, A., Phillips, J., & Menon, V. (2013). Default mode network in childhood autism: posteromedial cortex heterogeneity and relationship with social deficits. *Biological Psychiatry, 74*, 212–219.
Menon, V. (2011). Large-scale brain networks and psychopathology: a unifying triple network model. *Trends in Cognitive Science, 15*, 483–506.
Morillo, D. S., & Gross, N. (2013). Probabilistic neural network approach for the detection of SAHS from overnight pulse oximetry. *Medical and Biological Engineering and Computing, 51*, 305–315.
Mueller, S., Keeser, D., Samson, A. C., Kirsch, V., Blautzik, J., Grothe, M., et al. (2013). Convergent findings of altered functional and structural brain connectivity in individuals with high functioning autism: a multimodal MRI study. *PLoS One, 8*, e67329.
Muller, R. A., Shih, P., Keehn, B., Deyoe, J. R., Leyden, K. M., & Shukla, D. K. (2011). Underconnected, but how? A survey of functional connectivity MRI studies in autism spectrum disorders. *Cerebral Cortex, 21*, 2233–2243.
Muniz, A. M., Liu, H., Lyons, K. E., Pahwa, R., Liu, W., Nobre, F. F., et al. (2010). Comparison among probabilistic neural network, support vector machine and logistic regression for evaluating the effect of subthalamic stimulation in Parkinson disease on ground reaction force during gait. *Journal of Biomechanics, 43*, 720–726.
Murdaugh, D. L., Shinkareva, S. V., Deshpande, H. R., Wang, J., Pennick, M. R., & Kana, R. K. (2012). Differential deactivation during mentalizing and classification of autism based on default mode network connectivity. *PLoS One, 7*, e50064.
Murphy, K., Birn, R. M., Handwerker, D. A., Jones, T. B., & Bandettini, P. A. (2009). The impact of global signal regression on resting state correlations: are anti-correlated networks introduced? *NeuroImage, 44*, 893–905.
Nielsen, J. A., Zielinski, B. A., Fletcher, P. T., Alexander, A. L., Lange, N., Bigler, E. D., et al. (2013). Multisite functional connectivity MRI classification of autism: ABIDE results. *Frontiers in Human Neuroscience, 7*, 599.
Orru, G., Pettersson-Yeo, W., Marquand, A. F., Sartori, G., & Mechelli, A. (2012). Using support vector machine to identify imaging biomarkers of neurological and psychiatric disease: a critical review. *Neuroscience and Biobehavioral Reviews, 36*, 1140–1152.
Paakki, J. J., Rahko, J., Long, X., Moilanen, I., Tervonen, O., Nikkinen, J., et al. (2010). Alterations in regional homogeneity of resting-state brain activity in autism spectrum disorders. *Brain Research, 1321*, 169–179.
Palumbo, B., Fravolini, M. L., Nuvoli, S., Spanu, A., Paulus, K. S., Schillaci, O., et al. (2010). Comparison of two neural network classifiers in the differential diagnosis of essential tremor and Parkinson's disease by (123)I-FP-CIT brain SPECT. *European Journal of Nuclear Medicine and Molecular Imaging, 37*, 2146–2153.
Pan, G., Yan, G., Qiu, X., & Cui, J. (2011). Bleeding detection in wireless capsule endoscopy based on probabilistic neural network. *Journal of Medical Systems, 35*, 1477–1484.
Sankari, Z., & Adeli, H. (2011). Probabilistic neural networks for diagnosis of Alzheimer's disease using conventional and wavelet coherence. *Journal of Neuroscience Methods, 197*, 165–170.
Sato, J. R., Hoexter, M. Q., Oliveira, P. P., Jr., Brammer, M. J., Consortium, M. A., Murphy, D., et al. (2013). Inter-regional cortical thickness correlations are associated with autistic symptoms: a machine-learning approach. *Journal of Psychiatric Research, 47*, 453–459.
Sherrod, P. H. (2003). *DTREG manual*. http://www.dtreg.com/DTREG.pdf.
Specht, D. F. (1990). Probabilistic neural networks and the polynomial Adaline as complementary techniques for classification. *IEEE Transactions on Neural Network, 1*, 111–121.
Supekar, K., Uddin, L. Q., Khouzam, A., Phillips, J., Gaillard, W. D., Kenworthy, L. E., et al. (2013). Brain hyperconnectivity in children with autism and its links to social deficits. *Cell Reports, 5*, 738–747.
Tyszka, J. M., Kennedy, D. P., Paul, L. K., & Adolphs, R. (2014). Largely typical patterns of resting-state functional connectivity in high-functioning adults with autism. *Cerebral Cortex, 24*, 1894–1905.
Tzourio-Mazoyer, N., Landeau, B., Papathanassiou, D., Crivello, F., Etard, O., Delcroix, N., et al. (2002). Automated anatomical labeling of activations in SPM using a macroscopic anatomical parcellation of the MNI MRI single-subject brain. *NeuroImage, 15*, 273–289.
Ubeyli, E. D. (2008). Implementing eigenvector methods/probabilistic neural networks for analysis of EEG signals. *Neural Networks, 21*, 1410–1417.

Uddin, L. Q., Menon, V., Young, C. B., Ryali, S., Chen, T., Khouzam, A., et al. (2011). Multivariate searchlight classification of structural magnetic resonance imaging in children and adolescents with autism. *Biological Psychiatry, 70*, 833–841.

Uddin, L. Q., Supekar, K., Lynch, C. J., Khouzam, A., Phillips, J., Feinstein, C., et al. (2013a). Salience network-based classification and prediction of symptom severity in children with autism. *JAMA Psychiatry, 70*, 869–879.

Uddin, L. Q., Supekar, K., & Menon, V. (2010). Typical and atypical development of functional human brain networks: insights from resting-state FMRI. *Frontiers in Systems Neuroscience, 4*, 21.

Uddin, L. Q., Supekar, K., & Menon, V. (2013b). Reconceptualizing functional brain connectivity in autism from a developmental perspective. *Frontiers in Human Neuroscience, 7*, 458.

Van Dijk, K. R., Sabuncu, M. R., & Buckner, R. L. (2012). The influence of head motion on intrinsic functional connectivity MRI. *NeuroImage, 59*, 431–438.

Varol, E., Gaonkar, B., Erus, G., Schultz, R., & Davatzikos, C. (2012). Feature ranking based nested support vector machine ensemble for medical image classification. In *Proc IEEE Int Symp Biomed Imaging* (pp. 146–149).

Weng, S. J., Wiggins, J. L., Peltier, S. J., Carrasco, M., Risi, S., Lord, C., et al. (2010). Alterations of resting state functional connectivity in the default network in adolescents with autism spectrum disorders. *Brain Research, 1313*, 202–214.

Wiggins, J. L., Peltier, S. J., Ashinoff, S., Weng, S. J., Carrasco, M., Welsh, R. C., et al. (2011). Using a self-organizing map algorithm to detect age-related changes in functional connectivity during rest in autism spectrum disorders. *Brain Research, 1380*, 187–197.

Yendiki, A., Greve, D. N., Wallace, S., Vangel, M., Bockholt, J., Mueller, B. A., et al. (2010). Multi-site characterization of an fMRI working memory paradigm: reliability of activation indices. *NeuroImage, 53*, 119–131.